

Electroacupuncture Promotes Motor Function Recovery in MCAO/R Rats by Activating Astrocyte-Related PI3K/AKT Pathway

Xiao-Qing Zhang^{1,2,*†}, Yi-He Wang^{1,2,†}, Li Sun¹, Bao-Qiang Dong^{1,2}, Yue-Jiao Sui^{1,2}, Jia-Zi Dong^{1,2}, Yang Han^{1,2}

¹Liaoning University of Traditional Chinese Medicine, Shenyang, Liaoning, China

²Liaoning Provincial Major Laboratory of Acupuncture, Health Preservation and Rehabilitation, Shenyang, Liaoning, China

Received May 4, 2022
Revised May 5, 2022
Accepted August 11, 2022

Correspondence to

Xiao-Qing Zhang

Liaoning Provincial Major Laboratory of Acupuncture, Health Preservation and Rehabilitation, Shenyang, Liaoning, China

E-mail 29218902@qq.com

†These authors contributed to the work equally and should be regarded as co-first authors.

Background: Electroacupuncture (EA) is a widely used traditional Chinese medicine method to manage various diseases, including cerebral ischemia-reperfusion injury (CIRI). **Objectives:** We assessed the neuroprotective effects of EA and examined its mechanism in a rat model of the middle cerebral artery occlusion-reperfusion (MCAO/R). The gait analysis was performed to evaluate the neuroprotective effects. Western blot and immunohistochemistry assays were carried out to determine the molecular mechanisms of EA.

Methods: Male SD rats were randomly divided into the sham operation group, right MCAO/R group, and EA group. EA was administered every day (4/20 Hz, 10 min/1 d) at the following acupoints: Baihui (DU20), Yintang (EX-HN3), and Zusanli (ST36). Gait and motor function were analyzed from day 8 onward.

Results: The plantar support and balance coordination of MCAO/R rats decreased, and the cellular structure of the ischemic penumbra was unclear. EA improved the gait dynamics of the rats, adjusted the cell structure, further activated astrocytes, and increased the expression and phosphorylation of phosphoinositide 3-kinase/protein kinase B (PI3K/PKB or AKT).

Conclusion: EA promoted astrocyte-related effects in the rat model. Our findings suggest that the neuroprotective mechanism of EA may be related to the activation of the PI3K/AKT signaling pathway. The intervention enhanced brain protection and improved motor functions.

Keywords: Cerebral ischemia-reperfusion, Electroacupuncture, Astrocytes, PI3K/AKT

INTRODUCTION

Ischemic stroke is an acute cerebrovascular disease with high morbidity, mortality, and disability. Aging increases the incidence of stroke. Overall, ischemic stroke accounts for 87% of all strokes in this population [1]. Ischemic stroke is the second leading cause of death in adults [2]. When cerebral ischemia occurs, blood flow can be restored and recalculated by means of recombinant tissue plasminogen activator (R-tPA), but this process is often accompanied by reperfusion injury. Cerebral ischemia-reperfusion injury (CIRI) is characterized by an intensified inflammatory response, enhanced oxidative stress, and increased autophagy. R-tPA can only improve the patency of the patient's blood supply. It is difficult to effectively recover residual neurological functions and motor functions following injury.

Acupuncture attenuates a therapeutic role in cerebrovascular diseases by targeting the excitation of the trigeminal nerve and enhancement between the damaged cortex and white matter after a stroke [3,4]. Acupuncture has played an increasing role in the clinical treatment of cerebral ischemia, and is well-accepted in Asia, Europe, and the United States, as an alternative therapy [5-7]. Moreover, electroacupuncture (EA) therapy applies modern biological electrical stimulation to enhance the conduction effects compared with traditional acupuncture. Studies have shown that EA can effectively improve impaired neurological and motor functions of CIRI patients with uncoordinated limbs [8].

Traditional Chinese medicine theory believes the human brain functions through Du and Ren meridians. The Du meridian acts through the corticospinal cord transmission as an external reflection. Professor Xu established the "Tongdu

Tiaoshen needles therapy”, an alternative acupuncture treatment method for treating CIRI and its sequelae which integrates the Du meridian with the brain and the spirit. Clinical studies showed that this method can statistically reduce the National Institutes of Health Neurological Function scores by promoting the expression of microtubule-associated protein 1 light chain 3- II and autophagy-related proteins in patients. As a result, the clinical treatment total effective rate is improved [9]. Studies have also found that laser acupuncture at the acupoint, Baihui (DU20) can exert antioxidant effects, inhibit inflammatory responses, and improve cognitive impairment and motor dysfunction in the middle cerebral artery occlusion rat model [10]. EA at the DU20 point can inhibit the expression of N-methyl-D-aspartate receptor subtype 1 in the hippocampal CA1 region and protect the cognitive function of the middle cerebral artery occlusion-reperfusion (MCAO/R) rats [11]. In contrast, EA at the Shenting (DU24) and DU20 points can inhibit the Janus kinase 2/signal transducer and activator of transcription 3 signaling pathway, thereby, increasing the expression of postsynaptic density protein-95 and synuclein in the hippocampal CA1 region, and enhance synaptic plasticity [12]. Furthermore, EA at the Yintang (EX-HN3) and DU20 points can increase the expression of brain-derived neurotrophic factor tyrosine kinase B [13]. Stroke is often accompanied by limb dysfunctions and poor flexion. Studies have shown that EA at the Waiguan (SJ5) and Zusanli (ST36) points promoted the expression of microRNA-223, increased the number of neural stem cells, and improved the neurological functional defect score [14]. In this study, we selected the acupoints, DU20 (Du meridian), EX-HN3 (extraordinary acupoint on Du route line), and ST36 (Stomach meridian) according to the “*Tongdu Tiaoshen* needles therapy” method. The combination of these three acupoints in treating CIRI using EA has rarely been reported.

Phosphoinositide 3-kinase/Protein kinase B (PI3K/PKB or AKT), also known as the PI3K/AKT signaling pathway, plays a protective role in regulating cell proliferation and inhibiting apoptosis of the nerve cells in CIRI. Phosphorylated phospho-protein kinase B (p-AKT) can be used as a marker of its activation [15-17]. PI3K/AKT is involved in neuron protection of the Leonuri Herba total alkali in MCAO/R rats [18]. The PI3K/AKT pathway promotes the proliferation of astrocytes (AS) [19-21] and the expression of the glial fibrillary acidic protein (GFAP) a characteristic marker of AS through the protein complex pathway [22]. In turn, AS provides nutritional support, promotes angiogenesis, and contributes to the repair of neurological functions after an ischemic stroke [23]. EA exerts neuroprotective effects against ischemic strokes through the PI3K/AKT pathway [24]. To date, the mechanism by which AS is enhanced and activated via EA is unclear.

This study presented novel evidence supporting the AS activation-related PI3K/AKT signaling effects of EA at the acupoints, DU20, EX-HN3, and ST36 leading to improved gait dynamics in MCAO/R rats. This study contributes to the clinical understanding of the neuroprotective effects of EA and its essential mechanism.

MATERIALS AND METHODS

1. Animals

Fifty-five SPF male SD rats, each weighing 220 g (\pm 20 g), were purchased from Liaoning Changsheng Biotechnology, and raised in the Animal Experiment Center of Liaoning University of Traditional Chinese Medicine (SPF Experimental Center). The rats were kept at a temperature of 22°C, with 45% relative humidity.

2. Experimental method

1) Establish the MCAO/R rat model

The rats were divided into the sham operation group (sham group) and operation groups (including the right MCAO/R and EA groups) by the random number table method. Except for the sham group, the other groups were modified by Longa's line embolization method to prepare the MCAO/R model [25]. A 40 mm fishing line (2.86 mm in diameter) was polished smooth with sandpaper and reserved. Before modeling, the rat was weighed and anesthetized with 1% pentobarbital sodium (intraperitoneal injection of 4 mg/100 g). After anesthesia, a midline incision was made in the neck, exposing the right common carotid artery (CCA), the internal carotid artery (ICA), and the external carotid artery (ECA). CCA and ICA were clamped by an arterial clamp to fuse the ECA's branches. The stump was gently pulled downward, and cut with a 0.2 mm incision. The end of the prepared fishing line was gently pushed into the skull along the ICA through the CCA bifurcate, and advanced approximately 20 mm to reach the middle cerebral artery. After 2 h of embolization, the fishing line was pulled out to allow the blood to flow again. In the sham group (n = 13), only the CCA was exposed. The rats were only allowed to have water for the first 24 h after surgery. To determine if the model was successful, the awakened rats were scored for neurological dysfunction.

2) Model evaluation and screening

Longa's grade 5 scoring standard was used to evaluate the MCAO/R rat model conformance (Table 1). Sober scores, graded from 1 to 3, represented successful modeling. Gradings of 0 or 4 equated to model failure and these were excluded from the experiment. The MCAO/R rats were randomly divided into the model group (n = 12) and the EA

Table 1. Longa grade 5 scoring criteria for neurological functional defects

Grade 0	No neurological defect symptoms (exclude).
Grade 1	Mild nerve function defect, cannot be fully extended to the left side of the forelimbs (include).
Grade 2	Moderate neurological impairment, left forelimb flexion and adduction when walking, turning in left circles, lifting the rat tail, and hanging in the air (included).
Grade 3	Severe neurological impairment, unstable standing, leaning to the left when walking (included).
Grade 4	Inability to walk spontaneously, contracture, lethargy, and reduced level of consciousness (excluded).

group (n = 13).

3) EA stimulation

Acupoints, DU20, EX-HN3, and bilateral ST36, were selected to treat the EA group according to “Experimental Acupuncture” and the legal position method of anthropomorphic acupoints. The rats were fixed on the stainless steel net in a prone position with disposable ties. Local hair at the acupoints was removed to prevent the acupuncture needles from slipping. Acupuncture needles (Hwato, 0.16 mm × 25 mm) were inserted at the following acupoints, *Baihui* (DU20, the center of the parietal bone, inserted obliquely backward at a depth of 2 mm), *Yintang* (EX-HN3, between the two eyebrows, inserted obliquely backward at a depth of 1 mm), and *Zusanli* (ST36, the posterolateral side of the knee joint and approximately 5 mm below the small head of the fibula, vertically inserted at a depth of 7 mm). The handles of these acupuncture needles were connected to an acupuncture electrical stimulator. The parameters for EA were set to a dilatational wave frequency of 4 Hz/20 Hz and visualized as the needle body gently shaking. The first treatment commenced at 3 pm on the day of the model operation and EA was applied to each rat for 10 min. Subsequently, the same treatment was performed every day at 3 pm for 7 consecutive days. Rats in the sham and the model groups were restrained for the same time without EA intervention.

4) Gait analysis

Before modeling, the rats were trained so that they were familiar with the channels and were able to autonomously advance towards the box. Longa’s score was performed again after the EA treatment, and the CatWalk XT animal gait acquisition and analysis system (Noldus, Netherlands) was used to identify and analyze the limb movement function of the rats.

5) Tissue collection

After all the interventions, 1% sodium pentobarbital was injected for deep anesthesia. Some of the rats had their thoracic cavity cut open after abdominal anesthesia to expose the heart. Heparin sodium 0.2 ml, in 1% concentration, was

injected intravenously into the left heart, and aortic intubation was performed through the left ventricle. After fixation with vascular forceps, the right atrial appendage was cut open, followed by rapid washing with normal saline at 37°C (150 ml). Fixation with 250 ml precooled 4% paraformaldehyde at 4°C by alternating fast and then slow perfusion was performed [26]. The other rats underwent abdominal aorta blood sampling, and the brains were quickly removed on ice and stored at -80°C (Dw-hl388 ultra-low temperature storage tank, Meiling) after quick freezing with liquid nitrogen.

6) Hematoxylin and eosin staining (n = 6 in each group)

Brain tissues were embedded and fixed in paraffin. The specimens were sliced (HI 1210 ultra-thin slicer, Leica), baked, dewaxed, rehydrated, and then, stained with hematoxylin dyed for 10 min. After rinsing with water, the specimens were stained with eosin for 3 min, sealed with neutral resin, and observed under a microscope (DM2000 digital microscope, Leica).

7) ELISA analysis (n = 6 in each group)

Serum was obtained by centrifugation of the whole blood. The brain tissues (0.1 g) were retrieved from the EP tube, 900 µl of phosphorous buffer saline (PBS) was added, and then placed in an ice box. Tissue homogenate was obtained using a tissue grinder. Reagents were added step by step according to the manufacturer’s instructions (ELISA kit, Shanghai Enzyme-linked Biotechnology). The results were quickly read by the microplate reader (SpectraMax-M2, Scientz) after incubation.

8) Immunohistochemical staining (n = 6 rats for each group)

Paraffin sections were washed with PBS. Then, H₂O₂, inactivated endogenous enzymes, heated repair antigen, and BAS blocking solution, were added. Subsequently, rabbit anti-PI3K IgG (Santa Cruz) was added and the sections were incubated at 37° for 1 h. The sections were washed with PBS 3 times. Then, goat anti-rabbit IgG secondary antibody (goat anti-rabbit fluorescent antibody, Bioss) was added, and the sections were incubated at 37°C for 20 min. The sections were washed with PBS 4 times before DAB color rendering

at 37°C for 20 min. The sections were washed again with distilled water, dehydrated, and sealed with transparent resin. Brownish-yellow particles represented positive cells.

9) Western blot analysis (n = 6 rats for each group)

The brain tissue supernatant was obtained by centrifugation at 4°C (12000 r/20 min, TGL-16 high-speed desktop refrigerated centrifuge, Xiangyi). Protein concentration was quantified by the BCA method. Electrophoresis was performed and the specimen was placed in the ice box. The PVDF transfer membrane was sealed with 5% skim milk at room temperature for 1.5 h, and then the primary antibody diluted at 1:1000 was added for 4°C overnight (rabbit anti-Akt, Santa Cruz, and rabbit anti-p-Akt, Bioswamp). TBST was washed 3 times, 7 min each time. The secondary antibody diluted at 1:3000 was added and incubated for 2 h. The ECL exposure color solution was mixed with liquid A and liquid B in equal proportion, and the film was uniformly covered. After 2 min of reaction, the PVDF transfer membrane was put into the exposure instrument (ImageQuant 350, GE). GAPDH was used as the internal reference for detection, and the sham group was used as 1 for homogenization.

3. Statistical method

The animal data surveyor and analyst were blinded. All statistical analyses were performed using Statistical Product Service Solutions software (SPSS, version 23.0, IBM Corp., Armonk, NY, USA). The measurement data are shown as mean \pm standard deviation ($X \pm S$). Statistical significance between the groups was analyzed with one-way ANOVA and the SNK-Q method. $p < 0.05$ was considered statistically significant in all analyses.

RESULTS

1. EA treatment improved neurological function score

Longa's score is a classic neuro-functional evaluation. The results showed that EA improved the neurological functional defect scores in the MCAO/R rats (Fig. 1).

2. EA improved gait dynamics

Gait analysis is a method for detecting motor functions and the sensitivity of the limbs under ischemic stroke conditions. We used the CatWalk analysis system to determine the effect of EA on MCAO/R-induced gait irregularity.

We used color 3D models to show the paw-floor-contact strength and recorded variations on an isometric line. Our results showed that the EA group had stronger paw-floor-contact strength and more complete isometric force than the model group (Fig. 2).

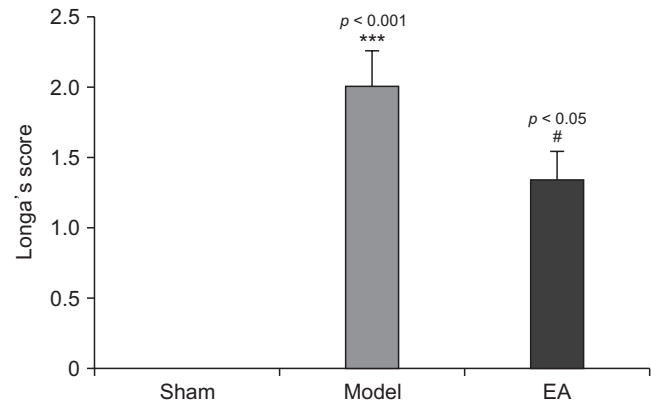


Fig. 1. The model group shows a higher Longa's score relative to the sham group ($p < 0.001$). The EA group shows a significantly lower Longa's score relative to the model group ($p < 0.05$). *** $p < 0.001$ # $p < 0.05$; n = 6 rats for each group).

We recorded the load changes experienced by marking each paw with different colors. Our result showed that the EA group had clearer and more complete footprints than the model group (Fig. 3).

As we know the maximum contact area reflects the degree of contact between the paws and the floor, and a larger contact area ensures more stable movement. Our result showed that the EA group had a larger maximum contact area than the model group. Maximum-contact-mean-intensity (MCMCI) is another indicator of motor functions. Our result showed that the MCMCI of the left paws increased in the EA group. Stride length is one of the motion parameters that reflect motion coordination. Our result showed that the EA group had longer stride lengths than the model group. Swing and swing speed are representative indicators of the swinging phase that reflect the stability of the motion posture. Our result showed that the EA group had shorter swing times and faster swing speeds than the model group (Fig. 4).

3. EA improved the tissue structures of the ischemic penumbra

We color-stained the nucleus and cytoplasm to observe the morphological and structural changes in the brain tissues. The results showed that the morphology of the brain tissues in the EA group was clear and more complete than in the model group. HE staining showed that the brain tissues of the sham group had clear morphological layers, no necrotic nerve cells, and were neatly structured. Edema, degeneration, atrophy, and necrosis of the nerve cells were observed in the model group with increased intercellular spacing. Compared with the model group, the morphological and structural disorders of the brain tissues in the EA group improved (Fig. 5).

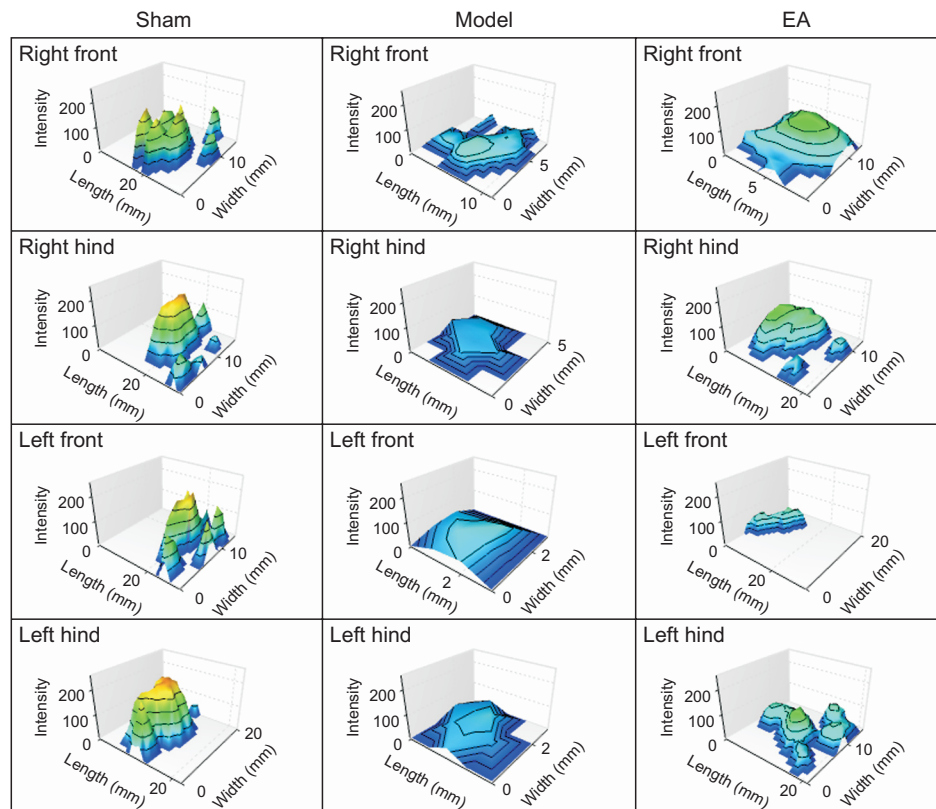


Fig. 2. Paw-floor-contact force in a colored 3D model to show the load changes experienced by the lower bearing. The sham group shows a stronger paw-braced force. Stereoscopic images show the height difference between the force isometric lines as large and circularly closed, which means the center of the paw and toes can be distinguished as the force is centripetally distributed. The model group shows a much weaker paw-braced force. There is no clear hierarchy between the force isometric lines and the lack of complete circular pattern, hence we could not distinguish the paw center from the tip of the toes. The EA group shows an enhanced paw-braced force relative to the model group. Its force isometric lines become rounder and more centralized. The color ranged from blue to green to yellow to red, indicating bearing strength from weak to strong. $n = 6$ rats for each group.

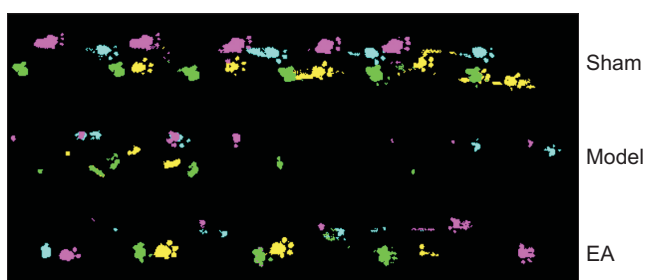


Fig. 3. Colored pawprint marks can visualize the load changes after EA treatment to MCAO/R rat model. The sham group: pawprints in maximal contact and intensity. The model group: pawprint can hardly be recognized and the intensity is minimal. The EA group: pawprints are coherent with recognizable contacts. Color marks: ① blue for right forepaw; ② purple for right hind paw; ③ yellow for left forepaw; ④ green for left hind paw; $n = 6$ rats for each group.

4. EA improved the GFAP content

Astrocytes (AS) can be found abundantly in the brain

tissues. GFAP is a type III intermediate filamentous protein exclusively found in AS and its expression level positively correlates with AS excitation [27]. This characteristic makes GFAP an exclusive marker of AS [28]. In other words, AS activation can be detected and determined by the GFAP content. Our data showed that AS activity in the EA group was higher than that in the model group. The ELISA results also confirmed the immunohistochemistry results. In sum, the GFAP content in the ischemic penumbra and serum of the EA group was higher than those in the model group. These findings suggest that EA can promote AS activation (Fig. 6).

5. EA increased the expression of the PI3K/AKT signaling pathway

Immunohistochemistry can reflect the expression of PI3K through the optical density value. Our results showed that the EA group had a more positive expression of PI3K than the model group (Fig. 7).

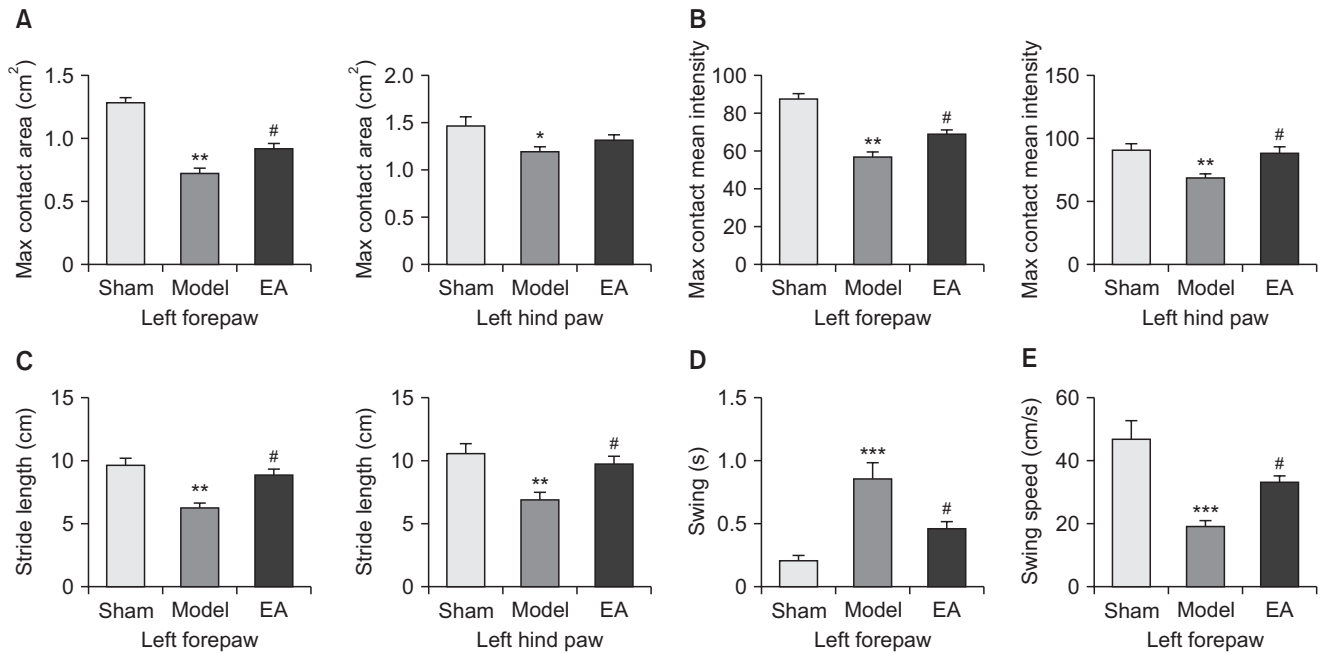


Fig. 4. EA's effect on the gait dynamics of MCAO/R rats. (A) The effect of EA at the DU20/EX-HN3/ST36 acupoints on the ipsilateral (left) paw-floor-contact area. The sham group (A, left) shows a smaller maximum forepaw-floor-contact area relative to the model group ($p < 0.01$), whereas the EA group (A, left) shows a forepaw-floor-contact area relative to the model group ($p < 0.01$). The sham group (A, right) shows a maximum hind paw-floor-contact area relative to the model group ($p < 0.05$); whereas, the EA group (A, right) shows a hind paw-floor-contact area relative to the model group but has no significant difference ($p > 0.05$). ** $p < 0.01$, * $p < 0.05$, # $p < 0.05$; $n = 6$ rats for each group. (B) The EA group's effect on the MCMI of the ipsilateral (left) paws of MCAO/R rats. The sham group (B, left) shows a strong forepaw-MCMI relative to the model group ($p < 0.01$). The EA group (B, left) shows a stronger forepaw-MCMI relative to the model group ($p < 0.05$). The sham group (B, right) shows a strong hind paw-MCMI relative to the model group ($p < 0.01$), whereas the EA group (B, right) shows a better hind paw-MCMI relative to the model group ($p < 0.05$). ** $p < 0.01$, # $p < 0.05$; $n = 6$ rats for each group. (C) The EA group's effect on the stride length of the ipsilateral (left) paws of MCAO/R rats. The sham group (C, left) shows a longer forepaw-stride-length relative to the model group ($p < 0.01$), whereas The EA group (C, left) shows a better forepaw-stride-length relative to the model group ($p < 0.05$). The sham group (C, right) shows a longer hind paw-stride-length relative to the model group ($p < 0.01$), whereas, the EA group (C, right) shows a better hind paw-stride-length relative to the model group ($p < 0.01$). ** $p < 0.01$, # $p < 0.05$; $n = 6$ rats for each group. (D) The EA group's effect on the swing time of the ipsilateral (left) paws of MCAO/R rats. The sham group shows a shorter forepaw swing time relative to the model group ($p < 0.001$). The EA group shows a shorter forepaw swing time relative to the model group ($p < 0.05$). *** $p < 0.001$, # $p < 0.05$; $n = 6$ rats for each group. (E) The EA group's effect on the swing speed of the ipsilateral (left) paws of MCAO/R rats. The sham group shows a faster forepaw swing speed relative to the model group ($p < 0.001$). The EA group shows a better forepaw swing speed relative to the model group ($p < 0.05$). *** $p < 0.001$, # $p < 0.05$; $n = 6$ rats for each group.

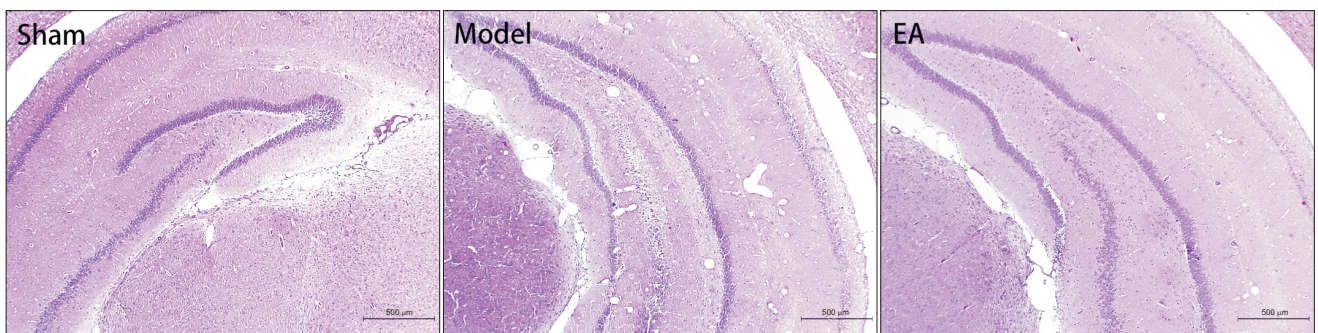


Fig. 5. HE staining of the ischemic penumbra (magnification $\times 20$). The sham group shows clear and orderly structured morphological layers with no necrotic nerve cells. Edema, degeneration, atrophy, and necrosis of the nerve cells with increased intercellular spacing are seen in the model group. The EA group shows an improved morphological and structural disorder of brain tissues. Color marks: ① bluish-purple for nucleus; ② red for cytoplasm. $n = 6$ rats for each group.

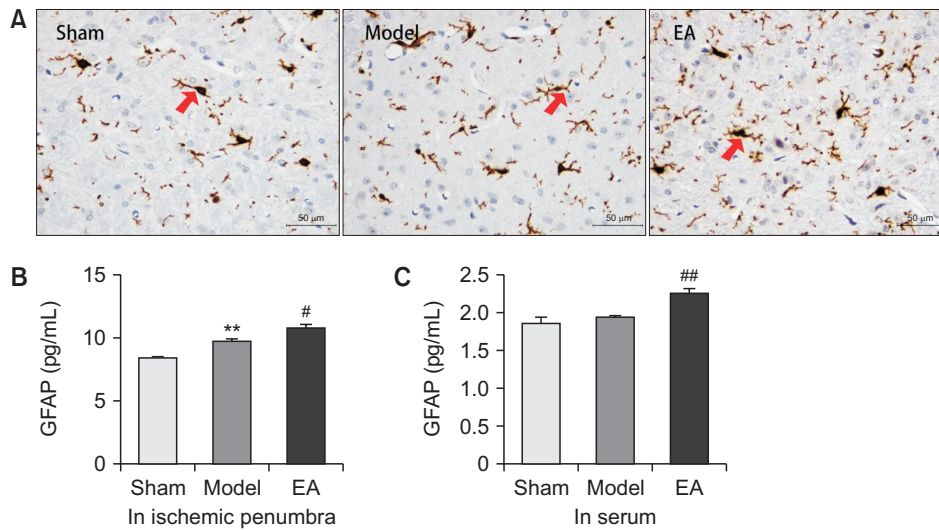


Fig. 6. EA treatment improved GFAP content (magnification $\times 200$). (A) Immunohistochemical staining of AS/GFAP expression in the cortex issues. AS can be seen in all of our cortex tissue samples. The sham group shows thin protrusions of the AS fibers with shallow staining. Compared with the sham group, the model group shows an enlarged AS cell body with increased protrusions and deepened staining. The EA group shows the increased expression of GFAP and the AS arrangement appears denser and more deeply stained ($n = 6$ rats for each group). (B) The GFAP content in the ischemic penumbra. The sham group shows a low GFAP content. The model group shows an increased GFAP content ($p < 0.01$) relative to the sham group. The EA group shows further increases in GFAP and AS ($p < 0.05$) relative to the model group. $**p < 0.001$, $^{\#}p < 0.05$; $n = 6$ rats for each group. (C) The serum GFAP content. The sham group shows a low GFAP content. The model group shows increased GFAP but the difference was not significant ($p > 0.05$). The EA group shows further increases in GFAP and AS ($p < 0.01$) relative to the model group. $^{\#\#}p < 0.01$; $n = 6$ rats for each group.

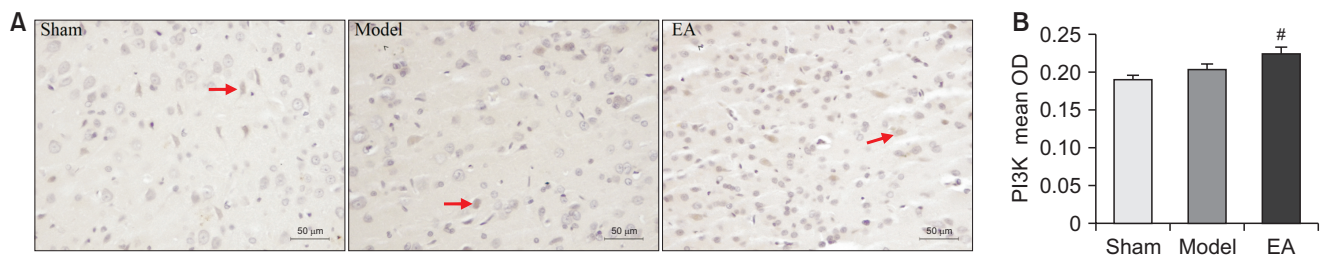


Fig. 7. PI3K expression observed by immunohistochemistry (magnification $\times 200$). (A) The sham group with some PI3K positive cells. The model Group shows an increased number of PI3K positive cells. The EA group shows more PI3K positive cells than the model group ($n = 6$ rats for each group). (B) The mean optical density of the PI3k positive cells. The model group shows a high expression of the PI3K protein relative to the sham group (not statistically significant). The EA group shows a higher expression of the PI3K protein relative to the model group ($p < 0.05$). $^{\#}p < 0.05$; $n = 6$ rats for each group.

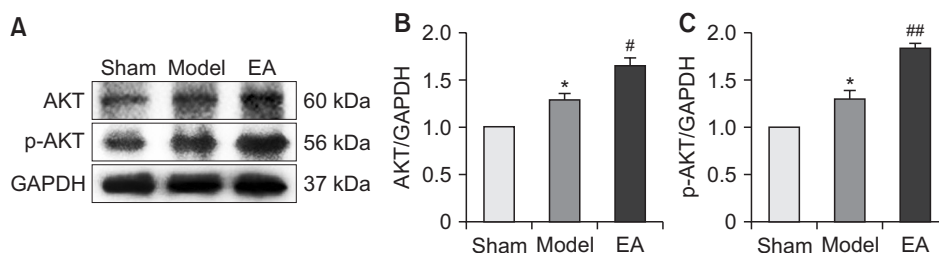


Fig. 8. Expression of AKT and p-AKT were detected by WB. (A) The sham group shows the blotting of the AKT proteins, while the p-AKT proteins were narrow and less expressed. The model group shows an increased expression of AKT and p-AKT. The EA group shows a higher expression of AKT and p-AKT relative to the model group ($n = 6$ rats for each group). (B, C) The relative expression levels of the AKT and p-AKT proteins. The model group (B) shows a high expression of the AKT and p-AKT proteins when compared to the sham group ($p < 0.05$). The EA group (B) shows a higher expression of the AKT and p-AKT protein relative to the model group ($p < 0.05$). The model group (C) shows a high expression of the AKT and p-AKT proteins relative to the sham group ($p < 0.05$). The EA group (C) shows a higher expression of the AKT and p-AKT proteins relative to the model group ($p < 0.01$). (B) AKT/GAPDH, (C) p-AKT/GAPDH; $^{\#\#}p < 0.01$, $^{\#}p < 0.05$, $^*p < 0.05$; $n = 6$ rats for each group.

AKT is the downstream protein of PI3K, and its increased expression can promote the recovery of the brain's structures and functions. The Western blot (WB) results showed that EA increased the expression and phosphorylation of AKT (Fig. 8).

DISCUSSION

Gait analysis is a method for detecting limb motor functions and limb sensitivity in patients with ischemic stroke. Therefore, we used the CatWalk gait analysis system to determine the effect of EA on MCAO/R-induced gait irregularity in a rat model. Gait analysis is commonly used to detect spinal cord and muscle injuries [29]. It was rarely used in CIRI-related experiments. Our study showed that CIRI behaviors can alter the step length, step speed, and other gait indicators. Our findings are consistent with the results of Barmann and Hetze's analysis of MCAO/R rats [30,31]. Moreover, the CatWalk analysis system can record the rats' movements, quantifying their complex and delicate motor abilities by identifying abnormal gait and determining its recovery. This is helpful for evaluating and screening effective treatment measures. Our data showed that MCAO/R rats demonstrated a slower swing speed, a longer swing time, and a shorter step length. The intensity and maximum paw-floor contact area of the affected forelimb were decreased, which concurred with Wang's findings [32]. Conversely, MCAO/R rats treated with EA showed an increase in their maximum plantar contact area, prolonged the step length, improved the swing speed, and reduced the swing time.

We used the acupoints, DU20, EX-HN3, and ST36, on MCAO/R rats to confirm EA's therapeutic effect on CIRI by improving the neural deficit scores and the cellular structure of the ischemic brain domain. The combining of these three acupoints was innovative. These points were selected carefully after evaluating the published CIRI intervention experiments that used Du20 and ST36 acupoints coupled with other acupoints, such as DU20 and DU24, PC6 and ST36, and LI11 and ST36 [33-35]. A dilatational-wave-mode stimulator was selected for our EA intervention. However, there were no consistent frequency parameters for us to use as experimental references. Therefore, we set the electrical needle stimulator at a frequency of 4 Hz/20 Hz by cross-referencing with Zou's 4 Hz/16 Hz [36] and Geng's 5 Hz/20 Hz [37]. Our results suggest that EA can activate nerve repair cytokines at the DU20, EX-HN3, and ST36 acupoints in MCAO/R rats.

Our study results showed that EA activated the PI3K/AKT pathway and increased the expression of GFAP (a characteristic marker of AS). The result was consistent with a published study using Geum Japonicum extracts to effectively treat CIRI through the PI3K/AKT pathway [38]. GFAP expression was not involved in the increase of infarct

volume after an ischemic stroke [39]. Studies have shown that EA at the *Neiguan* acupoint can increase GFAP and thus, improve the neurological functions of MCAO rats [40]. Our results showed that the nerve injury was effectively repaired, and the expression level of reactive astrocytes (RAS) was increased in the EA group. Our data also revealed lower Longa neurological function scores, enhanced HE staining of the hippocampal brain tissue structures, and improved gait test results. Considering these findings, RAS may play an essential role in nerve repair after ischemic brain injury.

The role of RAS has become controversial over time. Since AS may manifest hyperactively in the later stage or during the convalescence period, we speculated that AS proliferation and activation in different phases were diversified at post-CIR. In the early stages of ischemia (including the acute and subacute stages), the moderate proliferation of RAS can stimulate the secretion of basic fibroblast growth factor (bFGF), vascular endothelial growth factor (VEGF), etc. [41]. These cytokines are known to reduce neuronal damage and promote the repair and improvement of neurological functions [42,43]. Moreover, ischemia-induced RAS has the characteristics of neural stem cells and can transform into neurons [44]. On the contrary, overactivated RAS become swollen, and the cell protuberance becomes extended and connected to form a glial scar [45]. Many researchers have suggested that the glial scar limits nerve regeneration and axon extension after the inflammation responses subside [46], thus, is a negative factor. Conversely, a recent study published in *Nature* suggests that scar formation by RAS can also contribute to axonal regeneration in the central nervous system [47]. Removal of the glial scar did not promote central nervous system repairs [48]. Furthermore, targeted ablation of the glial scar may aggravate disease injury [49]. The recovery duration may influence the AS tendency toward positive versus negative effects. In terms of spatial distribution, whether the activation and distribution of AS vary at different brain domains has not been comprehensively concluded. Recent studies have suggested that AS activation and an increase in GFAP are beneficial in the early stage of CIRI [50]. In this study, all tests were performed on day 8 after the onset of the subacute phase of CIRI and our results support that RAS played an active role during this time. However, the specific CIR repair mechanism driven by AS, and its pattern of advantages and disadvantages, warrant further investigations.

CONCLUSIONS

This study proved that EA treatment at the acupoints of DU20, EX-HN3, and ST36 involved in the regulation of astrocyte activation-related PI3K/AKT signaling. And our data suggests that EA treatment can promote the recovery of

motor function in MCAO/R rats.

FUNDING

This work was supported by Department of Education of Liaoning Province, L202065.

ACKNOWLEDGEMENTS

This study was financially supported by the Department of Education of Liaoning Province (L202065) and the Liaoning Provincial Major Laboratory of Acupuncture, Health Preservation, and Rehabilitation.

AUTHORS' CONTRIBUTIONS

XQ Z provided experimental ideas. YH W was a major contributor in writing the manuscript. Li Sun provided suggestions on the improvement of the structure of the article. All authors read and approved the final manuscript.

ETHICAL STATEMENT

This experiment was approved by the Animal Ethics Review Committee of Liaoning University of Traditional Chinese Medicine and conducted in strict accordance with the 3R principle.

DATA AVAILABILITY

The data used to support the findings of this study are available from the corresponding author upon request.

CONFLICT OF INTEREST

The authors declare no conflict of interest.

ORCID

Xiao-Qing Zhang, <https://orcid.org/0000-0002-0521-8231>
 Yi-He Wang, <https://orcid.org/0000-0003-0794-6539>
 Li Sun, <https://orcid.org/0000-0002-6840-0575>
 Bao-Qiang Dong, <https://orcid.org/0000-0002-1250-210X>
 Yue-Jiao Sui, <https://orcid.org/0000-0002-7034-9756>
 Jia-Zi Dong, <https://orcid.org/0000-0002-1128-0234>
 Yang Han, <https://orcid.org/0000-0003-0262-803X>

REFERENCES

1. Saini V, Guada L, Yavagal DR. Global epidemiology of stroke and access to acute ischemic stroke interventions. *Neurology*

2021;97(20 Suppl 2):S6-16. <https://doi.org/10.1212/WNL.000000000012781>

2. Li Z, Cui Y, Feng J, Guo Y. Identifying the pattern of immune related cells and genes in the peripheral blood of ischemic stroke. *J Transl Med* 2020;18:296. <https://doi.org/10.1186/s12967-020-02463-0>
3. Han X, Bai L, Sun C, Niu X, Ning Y, Chen Z, et al. Acupuncture enhances communication between cortices with damaged white matters in poststroke motor impairment. *Evid Based Complement Alternat Med* 2019;2019:4245753. <https://doi.org/10.1155/2019/4245753>
4. Zhang ZJ, Wang XM, McAlonan GM. Neural acupuncture unit: a new concept for interpreting effects and mechanisms of acupuncture. *Evid Based Complement Alternat Med* 2012;2012:429412. <https://doi.org/10.1155/2012/429412>
5. Zhang BY, Wang GR, Ning WH, Liu J, Yang S, Shen Y, et al. Electroacupuncture pretreatment elicits tolerance to cerebral ischemia/reperfusion through inhibition of the GluN2B/m-calpain/p38 MAPK proapoptotic pathway. *Neural Plast* 2020;2020:8840675. <https://doi.org/10.1155/2020/8840675>
6. Li G, Li X, Dong J, Han Y. Electroacupuncture ameliorates cerebral ischemic injury by inhibiting ferroptosis. *Front Neurol* 2021;12:619043. <https://doi.org/10.3389/fneur.2021.619043>
7. Zhang S, Wu B, Liu M, Li N, Zeng X, Liu H, et al. Acupuncture efficacy on ischemic stroke recovery: multicenter randomized controlled trial in China. *Stroke* 2015;46:1301-6. <https://doi.org/10.1161/STROKEAHA.114.007659>
8. Wang C, Wu Z, Li N, Zhao Y, Tian F, Zhou X, et al. Clinical curative effect of electric acupuncture on acute cerebral infarction: a randomized controlled multicenter trial. *J Tradit Chin Med* 2014;34:635-40. [https://doi.org/10.1016/s0254-6272\(15\)30075-3](https://doi.org/10.1016/s0254-6272(15)30075-3)
9. Xu Q, Peng Y. [Clinical observation of “Tongdu Tiaoshen needles therapy” in treating acute cerebral infarction and its effect on autophagy]. *Zhongguo Zhen Jiu* 2018;38:4573-61. Chinese. <https://doi.org/10.13703/j.0255-2930.2018.05.001>
10. Jittiwat J. Baihui point laser acupuncture ameliorates cognitive impairment, motor deficit, and neuronal loss partly via anti-oxidant and anti-inflammatory effects in an animal model of focal ischemic stroke. *Evid Based Complement Alternat Med* 2019;2019:1204709. <https://doi.org/10.1155/2019/1204709>
11. Lin YW, Hsieh CL. Electroacupuncture at Baihui acupoint (GV20) reverses behavior deficit and long-term potentiation through N-methyl-d-aspartate and transient receptor potential vanilloid subtype 1 receptors in middle cerebral artery occlusion rats. *J Integr Neurosci* 2010;9:269-82. <https://doi.org/10.1142/s0219635210002433>
12. Xie G, Song C, Lin X, Yang M, Fan X, Liu W, et al. Electroacupuncture regulates hippocampal synaptic plasticity via inhibiting Janus-activated kinase 2/signal transducer and activator of transcription 3 signaling in cerebral ischemic rats. *J Stroke*

- Cerebrovasc Dis 2019;28:792-9. <https://doi.org/10.1016/j.jstroke-cerebrovasdis.2018.11.025>
13. Zheng Y, Qin Z, Tsoi B, Shen J, Zhang ZJ. Electroacupuncture on trigeminal nerve-innervated acupoints ameliorates post-stroke cognitive impairment in rats with middle cerebral artery occlusion: involvement of neuroprotection and synaptic plasticity. *Neural Plast* 2020;2020:8818328. <https://doi.org/10.1155/2020/8818328>
 14. Sha R, Han X, Zheng C, Peng J, Wang L, Chen L, et al. The effects of electroacupuncture in a rat model of cerebral ischemia-reperfusion injury following middle cerebral artery occlusion involves microRNA-223 and the PTEN signaling pathway. *Med Sci Monit* 2019;25:10077-88. <https://doi.org/10.12659/MSM.919611>
 15. Feng C, Wan H, Zhang Y, Yu L, Shao C, He Y, et al. Neuroprotective effect of Danhong injection on cerebral ischemia-reperfusion injury in rats by activation of the PI3K-Akt pathway. *Front Pharmacol* 2020;11:298. <https://doi.org/10.3389/fphar.2020.00298>
 16. Luan Q, Pan L, He D, Gong X, Zhou H. SC79, the AKT activator protects cerebral ischemia in a rat model of ischemia/reperfusion injury. *Med Sci Monit* 2018;24:5391-7. <https://doi.org/10.12659/MSM.910191>
 17. Zhou Z, Xu N, Matei N, McBride DW, Ding Y, Liang H, et al. Sodium butyrate attenuated neuronal apoptosis via GPR41/Gβγ/PI3K/Akt pathway after MCAO in rats. *J Cereb Blood Flow Metab* 2021;41:267-81. <https://doi.org/10.1177/0271678X20910533>
 18. Li Y, Xiang L, Wang C, Song Y, Miao J, Miao M. Protection against acute cerebral ischemia/reperfusion injury by Leonuri Herba Total Alkali via modulation of BDNF-TrkB-PI3K/Akt signaling pathway in rats. *Biomed Pharmacother* 2021;133:111021. <https://doi.org/10.1016/j.biopha.2020.111021>
 19. Wu CY, Yin KZ, Zhang Y, Jiao M, Zhao XY, Wu QY. 2,3,7,8-Tetrachlorodibenzo-p-dioxin promotes proliferation of astrocyte cells via the Akt/STAT3/cyclin D1 pathway. *Biomed Environ Sci* 2019;32:281-90. <https://doi.org/10.3967/bes2019.038>
 20. Zhang K, Wu S, Li Z, Zhou J. MicroRNA-211/BDNF axis regulates LPS-induced proliferation of normal human astrocyte through PI3K/AKT pathway. *Biosci Rep* 2017;37:BSR20170755. <https://doi.org/10.1042/BSR20170755>
 21. Endersby R, Zhu X, Hay N, Ellison DW, Baker SJ. Nonredundant functions for Akt isoforms in astrocyte growth and gliomagenesis in an orthotopic transplantation model. *Cancer Res* 2011;71:4106-16. <https://doi.org/10.1158/0008-5472.CAN-10-3597>
 22. Tripathi S, Kushwaha R, Mishra J, Gupta MK, Kumar H, Sanyal S, et al. Docosahexaenoic acid up-regulates both PI3K/AKT-dependent FABP7-PPARγ interaction and MKP3 that enhance GFAP in developing rat brain astrocytes. *J Neurochem* 2017;140:96-113. <https://doi.org/10.1111/jnc.13879>
 23. Sofroniew MV. Astrocyte reactivity: subtypes, states, and functions in CNS innate immunity. *Trends Immunol* 2020;41:758-70. <https://doi.org/10.1016/j.it.2020.07.004>
 24. Zheng T, Shi Y, Zhang J, Peng J, Zhang X, Chen K, et al. MiR-130a exerts neuroprotective effects against ischemic stroke through PTEN/PI3K/AKT pathway. *Biomed Pharmacother* 2019;117:109117. <https://doi.org/10.1016/j.biopha.2019.109117>
 25. Longa EZ, Weinstein PR, Carlson S, Cummins R. Reversible middle cerebral artery occlusion without craniectomy in rats. *Stroke* 1989;20:84-91. <https://doi.org/10.1161/01.str.20.1.84>
 26. Gage GJ, Kipke DR, Shain W. Whole animal perfusion fixation for rodents. *J Vis Exp* 2012;(65):3564.
 27. Shang Y, Gu PF, Yuan ST, Li Y, Gao G. Effects of dexmedetomidine on astrocytes glial fibrillary acidic protein expression in focal cerebral ischemia/reperfusion rats. *Chin J Mod Appl Pharm* 2015;32:799-803.
 28. Yang J, Zhang X, Chen X, Wang L, Yang G. Exosome mediated delivery of miR-124 promotes neurogenesis after ischemia. *Mol Ther Nucleic Acids* 2017;7:278-87. <https://doi.org/10.1016/j.omtn.2017.04.010>
 29. Timotius IK, Bieler L, Couillard-Despres S, Sandner B, Garcia-Ovejero D, Labombarda F, et al. Combination of defined CatWalk gait parameters for predictive locomotion recovery in experimental spinal cord injury rat models. *eNeuro* 2021;8:ENEURO.0497-20.2021. <https://doi.org/10.1523/ENEURO.0497-20.2021>
 30. Bärmann J, Walter HL, Pikhovych A, Endepols H, Fink GR, Rueger MA, et al. An analysis of the CatWalk XT and a composite score to assess neurofunctional deficits after photothrombosis in mice. *Neurosci Lett* 2021;751:135811. <https://doi.org/10.1016/j.neulet.2021.135811>
 31. Hetze S, Römer C, Teufelhart C, Meisel A, Engel O. Gait analysis as a method for assessing neurological outcome in a mouse model of stroke. *J Neurosci Methods* 2012;206:7-14. <https://doi.org/10.1016/j.jneumeth.2012.02.001>
 32. Wang Y, Bontempi B, Hong SM, Mehta K, Weinstein PR, Abrams GM, et al. A comprehensive analysis of gait impairment after experimental stroke and the therapeutic effect of environmental enrichment in rats. *J Cereb Blood Flow Metab* 2008;28:1936-50. <https://doi.org/10.1038/jcbfm.2008.82>
 33. Chen B, Lin WQ, Li ZF, Zhong XY, Wang J, You XF, et al. Electroacupuncture attenuates ischemic brain injury and cellular apoptosis via mitochondrial translocation of cofilin. *Chin J Integr Med* 2021;27:705-12. <https://doi.org/10.1007/s11655-021-3335-4>
 34. Lü K, Li F, Gong B, Dai EZ, Wang Y, Zeng ZH. [Effect of electroacupuncture of "Neiguan" (PC 6) and "Zusanli" (ST 36) on expression of cerebral cortical slit 2/Robo 1 in the focal cerebral infarction rats]. *Zhen Ci Yan Jiu* 2013;38:265-70. Chinese.
 35. Tao J, Chen B, Gao Y, Yang S, Huang J, Jiang X, et al. Electroacupuncture enhances hippocampal NSCs proliferation in

- cerebral ischemia-reperfusion injured rats via activation of notch signaling pathway. *Int J Neurosci* 2014;124:204-12. <https://doi.org/10.3109/00207454.2013.840781>
36. Zou J, Huang GF, Xia Q, Li X, Shi J, Sun N. Electroacupuncture promotes microglial M2 polarization in ischemic stroke via annexin A1. *Acupunct Med* 2022;40:258-67. <https://doi.org/10.1177/09645284211057570>
 37. Geng Y, Chen Y, Sun W, Gu Y, Zhang Y, Li M, et al. Electroacupuncture ameliorates cerebral I/R-induced inflammation through DOR-BDNF/TrkB pathway. *Evid Based Complement Alternat Med* 2020;2020:3495836. <https://doi.org/10.1155/2020/3495836>
 38. Ou B, Tao W, Yang S, Feng J, Wang J, Yang T, et al. The antiapoptosis effect of *Geum japonicum* Thunb. var. *chinense* extracts on cerebral ischemia reperfusion injury via PI3K/Akt pathway. *Evid Based Complement Alternat Med* 2018;2018:7290170. <https://doi.org/10.1155/2018/7290170>
 39. Zheng Z, Yi X, Lv J. Loss of GFAP and vimentin does not affect peri-infarct depolarizations after focal cerebral ischemia. *Eur Neurol* 2020;83:301-9. <https://doi.org/10.1159/000507990>
 40. Zhao H, Lu Y, Wang Y, Han X, Zhang Y, Han B, et al. Electroacupuncture contributes to recovery of neurological deficits in experimental stroke by activating astrocytes. *Restor Neurol Neurosci* 2018;36:301-12. <https://doi.org/10.3233/RNN-170722>
 41. Liu Z, Chopp M. Astrocytes, therapeutic targets for neuroprotection and neurorestoration in ischemic stroke. *Prog Neurobiol* 2016;144:103-20. <https://doi.org/10.1016/j.pneurobio.2015.09.008>
 42. Jha MK, Seo M, Kim JH, Kim BG, Cho JY, Suk K. The secretome signature of reactive glial cells and its pathological implications. *Biochim Biophys Acta* 2013;1834:2418-28. <https://doi.org/10.1016/j.bbapap.2012.12.006>
 43. Magnusson JP, Göritz C, Tatarishvili J, Dias DO, Smith EM, Lindvall O, et al. A latent neurogenic program in astrocytes regulated by Notch signaling in the mouse. *Science* 2014;346:237-41. <https://doi.org/10.1126/science.1246.6206.237>
 44. Yang W, Shen Y, Chen Y, Chen L, Wang L, Wang H, et al. Mesencephalic astrocyte-derived neurotrophic factor prevents neuron loss via inhibiting ischemia-induced apoptosis. *J Neurol Sci* 2014;344:129-38. <https://doi.org/10.1016/j.jns.2014.06.042>
 45. Cekanaviciute E, Fathali N, Doyle KP, Williams AM, Han J, Buckwalter MS. Astrocytic transforming growth factor-beta signaling reduces subacute neuroinflammation after stroke in mice. *Glia* 2014;62:1227-40. <https://doi.org/10.1002/glia.22675>
 46. Bramlett HM, Dietrich WD. Pathophysiology of cerebral ischemia and brain trauma: similarities and differences. *J Cereb Blood Flow Metab* 2004;24:133-50. <https://doi.org/10.1097/01.WCB.0000111614.19196.04>
 47. Anderson MA, Burda JE, Ren Y, Ao Y, O'Shea TM, Kawaguchi R, et al. Astrocyte scar formation aids central nervous system axon regeneration. *Nature* 2016;532:195-200. <https://doi.org/10.1038/nature17623>
 48. Williamson MR, Fuertes CJA, Dunn AK, Drew MR, Jones TA. Reactive astrocytes facilitate vascular repair and remodeling after stroke. *Cell Rep* 2021;35:109048. <https://doi.org/10.1016/j.celrep.2021.109048>
 49. Adams KL, Gallo V. The diversity and disparity of the glial scar. *Nat Neurosci* 2018;21:9-15. <https://doi.org/10.1038/s41593-017-0033-9>
 50. Zamanian JL, Xu L, Foo LC, Nouri N, Zhou L, Giffard RG, et al. Genomic analysis of reactive astrogliosis. *J Neurosci* 2012;32:6391-410. <https://doi.org/10.1523/JNEUROSCI.6221-11.2012>